Viral Polymerase-Helicase Complexes Regulate Replication Fidelity To Overcome Intracellular Nucleotide Depletion

Kenneth A. Stapleford,[a] Kathryn Rozen-Gagnon,[a*] Pratyush Kumar Das,[b] Sirle Saul,[b] Enzo Z. Poirier,[a] Hervé Blanc,[a] Pierre-Olivier Vidalain,[c*] Andres Merits,[b] Marco Vignuzzi[a]

Institut Pasteur, Viral Populations and Pathogenesis Unit, Centre National de la Recherche Scientifique UMR 3569, Paris, France[a]; Institute of Technology, University of Tartu, Tartu, Estonia[b]; Institut Pasteur, Unité de Génomique Virale et Vaccination, Centre National de la Recherche Scientifique UMR 3569, Paris, France[c]

ABSTRACT

To date, the majority of work on RNA virus replication fidelity has focused on the viral RNA polymerase, while the potential role of other viral replicase proteins in this process is poorly understood. Previous studies used resistance to broad-spectrum RNA mutagens, such as ribavirin, to identify polymerases with increased fidelity that avoid misincorporation of such base analogues. We identified a novel variant in the alphavirus viral helicase/protease, nonstructural protein 2 (nsP2) that operates in concert with the viral polymerase nsP4 to further alter replication complex fidelity, a functional linkage that was conserved among the alphavirus genus. Purified chikungunya virus nsP2 presented delayed helicase activity of the high-fidelity enzyme, and yet purified replication complexes manifested stronger RNA polymerization kinetics. Because mutagenic nucleoside analogs such as ribavirin also affect intracellular nucleotide pools, we addressed the link between nucleotide depletion and replication fidelity by using purine and pyrimidine biosynthesis inhibitors. High-fidelity viruses were more resistant to these conditions, and viral growth could be rescued by the addition of exogenous nucleosides, suggesting that mutagenesis by base analogues requires nucleotide pool depletion. This study describes a novel function for nsP2, highlighting the role of other components of the replication complex in regulating viral replication fidelity, and suggests that viruses can alter their replication complex fidelity to overcome intracellular nucleotide-depleting conditions.

IMPORTANCE

Previous studies using the RNA mutagen ribavirin to select for drug-resistant variants have highlighted the essential role of the viral RNA-dependent RNA polymerase in regulating replication fidelity. However, the role of other viral replicase components in replication fidelity has not been studied in detail. We identified here an RNA mutagen-resistant variant of the nsP2 helicase/protease that conferred increased fidelity and yet could not operate in the same manner as high-fidelity polymerases. We show that the alphavirus helicase is a key component of the fidelity-regulating machinery. Our data show that the RNA mutagenic activity of compounds such as ribavirin is coupled to and potentiated by nucleotide depletion and that RNA viruses can fine-tune their replication fidelity when faced with an intracellular environment depleted of nucleotides.

R NA viruses rapidly generate large amounts of genetic diversity, all while maintaining genomic integrity, processes which have thus far been essentially restricted to the function of the polymerase. Little is known regarding other viral or cellular components that might regulate fidelity, and in particular those involved in alphavirus replication. By using RNA mutagens to alter mutation rates, the fidelity determinants within the viral polymerase of many RNA viruses have been identified, including foot-and-mouth disease virus (1, 2), poliovirus (3, 4), Coxsackie B virus (5, 6), influenza A virus (7), human enterovirus 71 (8, 9), chikungunya virus (CHIKV) (10, 11), and Sindbis virus (SINV) (11). Mutagenic compounds such as ribavirin and 5-fluorouracil are base analogs that provoke mutations in downstream replication cycles after they are misincorporated into the genome. However, ribavirin also functions as an IMP dehydrogenase (IMPDH) inhibitor, an enzyme necessary for *de novo* purine biosynthesis and more specifically intracellular GTP levels (12–15), whereas 5-fluorouracil inhibits thymidylate synthase, leading to decreases in dTTP and increases in dUTP (16) and thus another imbalance in nucleotide pools. Thus, in addition to avoiding the incorporation of mutagenic base analogs, resistance may arise to overcome imbalances in nucleotide pools. How such resistance could be

achieved and whether such variants would present altered fidelity is not known.

CHIKV is an alphavirus and member of the *Togaviridae* family. CHIKV is an enveloped positive-strand RNA virus containing an 11.8-kb genome which encodes 10 gene products during viral replication. These include four nonstructural proteins (nsP1 to nsP4) required for RNA replication and six structural proteins (capsid, E3, E2, 6K, TF, and E1) necessary for virion production (17). Of the nonstructural proteins, nsP1 contributes to membrane binding, capping events since the viral guanylyl- and methyltransferase and is also required for negative-strand RNA synthesis (18); nsP2 is a multifunctional protein which exhibits helicase, NTPase, and protease activity, as well as carries a carboxy-terminal putative methyltransferase-like domain (19–22). In addition to roles in precise viral polyprotein cleavage and processing during the initial steps in replication, nsP2 is also required for cellular transcriptional shutoff during infection (22–24). nsP3 harbors macrodomains, zinc binding domains, and a hypervariable region, whereas nsP4 is the viral RNA-dependent RNA polymerase (RdRp) (25). These four nonstructural proteins, along with host cofactors, function together to orchestrate efficient genome replication (20).

Similar to other studies, we previously utilized the RNA mutagens ribavirin and 5-fluorouracil to study drug-resistant mutations in alphaviruses (CHIKV and SINV) and identified residue 483 of the RdRp nsP4 as a key determinant of polymerase fidelity (10, 11). Interestingly, in the initial screen for drug-resistant variants (10), we identified an additional variant of the nsP2 protein that was not further characterized. In the present study, we found this nsP2 variant G641D was resistant to RNA mutagens and increased fidelity through a mechanism independent of the viral polymerase. In addition, biochemical assays showed that high-fidelity nsP2 had reduced helicase activity, whereas isolated high-fidelity replication complexes increased replication kinetics and resistance to low nucleotide concentrations. Finally, we found the high-fidelity variants to be resistant to other nucleotide biosynthesis inhibitors, such as mycophenolic acid and brequinar, suggesting that these variants were selected due to their ability to utilize and survive in low or imbalanced nucleotide conditions. Taken together, these data provide a novel role for nsP2 in regulating alphavirus fidelity and expand our knowledge on other viral components required to regulate these processes. In addition, our results show that RNA viruses can alter their biology to regulate replication fidelity as the intracellular environment changes.

MATERIALS AND METHODS

Cells and viruses. The mammalian Vero, HeLa, and BHK-21 cell lines were maintained in Dulbecco modified Eagle medium (DMEM; Gibco) supplemented with 10% newborn calf serum (Gibco) and 1% penicillin-streptomycin (Sigma) at 37°C with 5% CO_2.

Wild-type (WT) CHIKV was generated from the La Reunion strain 06-049 infectious clone, as previously described (10). CHIKV nsP2 and nsP4 mutants were generated by site-directed mutagenesis of the infectious clone using the QuikChange II XL site-directed mutagenesis kit (Stratagene). All newly generated DNA plasmids were Sanger sequenced in full (GATC Biotech) to confirm mutagenesis and to that ensure no second-site mutations were introduced. The SINV nsP2 mutant was constructed in the same fashion from the pTR339 wild-type infectious clone (26). Plasmids containing cDNAs of CHIKV and SINV infectious clones were linearized with NotI or XhoI, respectively, purified by phenol-chloroform extraction and ethanol precipitation, and subsequently used for *in vitro* transcription of viral RNAs using the SP6 mMESSAGE mMACHINE

kit (Ambion). RNAs were then purified by phenol-chloroform extraction and ethanol precipitation, quantified, diluted to 1 μg/μl, and stored at −80°C.

For RNA transfections, BHK-21 cells were treated with trypsin, washed twice with ice-cold phosphate-buffered saline (PBS), and resuspended at a concentration of 2×10^7 cells/ml in ice-cold PBS. Cells (0.390 ml) were mixed with 10 μg of *in vitro*-transcribed viral RNA, placed in a 2-mm gap cuvette, and electroporated at 1.2 kV and 25 μF with infinite Ω in an XCell gene pulser (Bio-Rad). Cells were allowed to recover for 10 min at room temperature and then mixed with 6 ml of prewarmed medium and placed into a T-25 flask. After 48 h of incubation at 37°C, virus titers were determined by standard plaque assay. In brief, 10-fold serial dilutions of each virus in DMEM were incubated on a confluent monolayer of Vero cells for 1 h at 37°C. After incubation, the cells were overlaid with 0.8% agarose dissolved in DMEM and 2% newborn calf serum, followed by incubation at 37°C for 72 h. The cells were then fixed with 4% formalin, the agarose plugs were removed, and plaques were visualized by the addition of crystal violet.

To generate working viral stocks, each virus sample was passaged once over a 70 to 80% confluent monolayer of BHK-21 cells, the titers were determined as described above, and the samples were divided into aliquots and stored at −80°C until use. All viruses were passaged three times in BHK-21 cells and fully sequenced to ensure mutation stability and no second-site mutations.

Drug sensitivity assays. HeLa cells (250,000 cells/well in 12-well tissue culture plates) were pretreated with either medium containing no drug or medium containing drugs (RNA mutagens or nucleotide biosynthesis inhibitors). The incubation times and concentrations were as follows: 2 h with 200 or 400 μM ribavirin and 5-fluorouracil (Sigma) at 40 μg/ml and 30 min with 0.5 μM brequinar and 20 μM mycophenolic acid (Sigma). Posttreatment, the medium was removed, and the cells were inoculated with virus in DMEM at a multiplicity of infection (MOI) of 0.1 for 1 h at 37°C. After virus incubation, medium containing each compound was added, and the cells were incubated for 72 h at 37°C. Virus was harvested at 72 h, and mean titers were obtained by determining the 50% tissue culture infective dose(s) ($TCID_{50}$). In brief, a 96-well tissue culture plates was plated for each virus with 10^4 Vero cells/well. Viruses were serially diluted in 8 10-fold dilutions in DMEM. Each dilution was distributed in a row of the 96-well plate, with each well receiving 100 μl of diluted virus. Viruses and cells were incubated 5 to 7 days at 37°C with 5% CO_2. After incubation, the cells were fixed with 50 μl of 4% formalin, the medium was removed, and 50 μl of crystal violet was added to each well. For ribavirin sensitivity assays, viruses that exhibited significant sensitivity or resistance compared to the wild type at $P < 0.05$ or greater at either 200 or 400 μM ribavirin were considered potential fidelity variants, and mutation frequencies were estimated.

Mutation frequencies by molecular cloning. To determine mutation frequencies, all mutants were electroporated in tandem into BHK-21 cells. Supernatants were collected 48 h later, and viral RNA was extracted as described above. For CHIKV, an ~800-bp region corresponding to nucleotides 9943 to 10726 was amplified of the E1 region of the genome using the forward primer 5′-TACGAACACGTAACAGTGATCC-3′ and the reverse primer 5′-CGCTCTTACCGGGTTTGTTG-3′. For SINV, the analogous region was amplified using the forward primer 5′-TACGAAC ATGCGACCACTGTTC-3′ and the reverse primer 5′-CGCTCGGAGCG GATTTACTG-3′, and ~500 bases of this fragment were included in the analysis. Amplified fragments were purified as described above, and 3 μl of each product was modified by a 3′ A-overhang addition reaction (1 μl of AmpliTaq Gold 10× buffer, 1 μl of 10 mM dATP). Modified products were cloned using the TopoTA cloning kit (Invitrogen), and single colonies were picked for sequencing. Mutation frequencies were determined as previously described (27). Mutation frequencies from HeLa and Vero cells were performed in a similar manner.

Population diversity and mutation frequencies by deep sequencing. To estimate the population diversity of variants by deep sequencing,

cDNA libraries were prepared using Maxima H Minus reverse transcriptase (Invitrogen) from RNA extracted from virus generated and passaged three times in BHK-21 cells. The viral genome was PCR amplified by using a high-fidelity polymerase (Phusion) to generate one amplicon spanning the majority of the CHIKV genome. PCR products were fragmented (Fragmentase), multiplexed, clustered, sequenced in the same lane with Illumina cBot and GAIIX technology, and analyzed with established deep-sequencing data analysis tools and in-house scripts. Briefly, per-base Phred quality scores were utilized to trim bases with error probabilities higher than 0.001, and sequences with fewer than 16 bases after trimming were discarded. For this purpose, we used the fastq-mcf tool from the ea-utils toolkit (http://code.google.com/p/ea-utils). The alignment step is performed using the Burrows-Wheeler Aligner (28), and Pileup analysis is performed using SAMtools (29). Once the pileup is done, the ViVAn bioinformatics pipeline was used to collect the data per position and calculate the variance at each nucleotide position by root mean square deviation (30). These values were then used to determine the mean variances and standard errors across the whole genome.

Viral replication and extracellular RNA synthesis. Virus growth was evaluated in BHK-21 cells, and titers were determined by calculating the $TCID_{50}$ for Vero cells as described above. Viruses were diluted to achieve an MOI of 1 in serum-free medium and incubated on each cell type for 1 h at 37°C. After this incubation, the virus was removed, the cells were washed twice in PBS, and complete medium was added. At 0, 2, 4, 8, and 24 h postinfection, supernatants were collected for titration and RNA extraction.

For CHIKV, the genome copy number was determined by extracting viral RNA from the supernatant at each time point using the TRIzol reagent and performing quantitative reverse transcription-PCR (qRT-PCR) using the TaqMan RNA-to-Ct kit (Applied Biosystems). Cycle threshold (C_T) values were determined in duplicate based on amplification of nsP4 transcripts using forward (5′-TCACTCCCTGCTGGACTTGATAGA-3′) and reverse (5′-TGACGAACAGAGTTAGGAACATACC-3′) primers and a probe (5′-[6-FAM] AGGTACGCGCTTCAAGTTCGGCG-3′) as previously published (31, 32). Standard curves were performed in each run using samples of *in vitro*-transcribed CHIKV RNA.

Pulse-chase analysis. BHK-21 cells were infected with wild-type CHIKV of the nsP2 G641D variant at an MOI of 10 in infection medium comprised of Glasgow minimum essential medium, 1% penicillin-streptomycin, 20 mM HEPES (pH 7.2), and 0.2% bovine serum albumin. At 3 h postinfection the cells were washed with starvation medium (methionine- and cysteine-free DMEM [Life Technologies] 20 mM HEPES [pH 7.2]) and incubated in starvation medium for 30 min at 37°C. After starvation, the medium was replaced with starvation medium containing 50 μCi of [³⁵S]methionine-cysteine mixture (Perkin-Elmer) for 15 min, followed by the addition of chase medium (starvation medium containing 10 mM methionine and 5 mM cysteine). At times 0, 15, and 45 min postchase, the cells were washed with PBS, lysed in 1% sodium dodecyl sulfate (SDS), boiled for 3 min, passed through a small gauge needle, and centrifuged for 5 min at 12,000 rpm. For immunoprecipitation, clarified lysate was diluted into NET 150 buffer (50 mM Tris [pH 8.0], 150 mM NaCl, 5 mM EDTA [pH 8.0], 1% Igepal), precleared with protein A-Sepharose (Sigma) for 1 h. Antibodies to CHIKV nsP1 and nsP2 were then added, and the samples were incubated overnight at 4°C. After antibody incubation, protein A-Sepharose was added for 1 h, and the beads were pelleted by centrifugation, washed three times with NET 400 buffer (50 mM Tris [pH 8.0], 400 mM NaCl, 5 mM EDTA [pH 8.0], 1% Igepal), and resuspended in 1× Laemmli buffer. Proteins were denatured by boiling for 10 min and separated on an 8% SDS-PAGE gel. Gels were fixed in Destain solution (45% methanol, 10% acetic acid), washed with H_2O, dried, vacuum dried, exposed to a phosphoscreen, and visualized using a Typhoon Trio scanner (GE Healthcare). The images were quantified using ImageJ.

Subcellular fractionation and immunoblotting. BHK-21 cells were infected with wild-type CHIKV, nsP4 C483Y, nsP2 G641D, and the double mutant at an MOI of 1 and then incubated at 37°C for 16 h. The medium was then removed, and the cells were washed once with PBS and treated with trypsin. The cells were harvested by centrifugation at 1,200 × *g* for 5 min, the supernatant was removed, and the cells were washed once with ice-cold PBS. Cells were resuspended in swelling buffer (10 mM Tris-HCl [pH 7.4], 10 mM NaCl, and 1.5 mM $MgCl_2$ containing complete protease inhibitor [Roche]), incubated on ice for 15 min, and lysed by Dounce homogenization. Homogenized samples were centrifuged at 500 × *g* for 5 min at 4°C. The supernatant was removed and centrifuged at 12,000 × *g* for 15 min at 4°C. Samples containing membrane fractions were resuspended in storage buffer (250 mM sucrose, 10 mM Tris-HCl [pH 7.4], 10 mM NaCl, complete protease inhibitor), and the total protein concentration was determined by Bradford Assay (Bio-Rad). Membrane fractions were adjusted to 5 mg of total protein/ml, divided into aliquots, and stored at −80°C.

For immunoblotting, samples were mixed with 2× Laemmli buffer (Bio-Rad) containing 10% 2-mercaptoethanol. Samples were heated at 95°C for 10 min, separated by SDS-PAGE and transferred to nitrocellulose membrane (Bio-Rad). Membranes were blocked in 5% nonfat milk in Tris-buffered saline (20 mM Tris-HCl [pH 7.4], 0.1 mM EDTA, 150 mM NaCl) containing 0.1% Tween 20 (TBST) and incubated overnight with antibodies to nsP1, nsP2, nsP3, or nsP4. Capsids prepared either in-house (E1 [kindly provided by P. Gorman]) or obtained from commercial sources (CoxIV; Cell Signaling; tubulin, Sigma) were diluted in blocking buffer. Membranes were washed extensively in TBST, incubated in secondary anti-rabbit horseradish peroxidase-antibody (Millipore), and washed three more times in TBST. Membranes were developed using Supersignal West Pico chemiluminescent substrate (Thermo Scientific).

Purification of CHIKV nsP2 variant. The nsP2 G641D mutation was introduced into the pET-nsP2 expression vector by site-directed mutagenesis using the primers described above. The expression and purification of wild-type nsP2, nsP2 G641D, and nsP2 5A-PG as a negative control (21) was performed as previously described (33). Bacterial cells were harvested from overnight culture and suspended in lysis buffer. After lysing the cells using a French press, the lysate was clarified by high-speed centrifugation. Subsequently, the proteins were purified by Ni affinity, ion exchange, and size exclusion, as described previously (33). The purity of the recombinant proteins was analyzed by standard PAGE. After the concentration of the protein samples was measured by a NanoDrop 1000 (Thermo Scientific), taking into consideration the extinction coefficient, the samples were flash frozen and stored at −80°C. Then, 1.5 μg of purified wild-type (WT) or G641D nsP2 enzymes was analyzed by SDS-PAGE (see Fig. 4B). Circular dichroism spectroscopy was performed as previously described (33) to ensure that the WT and variant nsP2 had comparable fold patterns (33).

CHIKV nsP2 *in vitro* protease cleavage assay. The substrates for nsP2 cleavage were designed and purified as previously described (21). Protein cleavage assays were carried out by incubating 250 ng of purified nsP2 or nsP2 G641D variant with 2 μg of substrate in assay buffer (20 mM HEPES [pH 7.2] and 2 mM dithiothreitol [DTT]) at a final volume of 8 μl. Reaction mixtures were incubated at 30°C for 6 min or 1 h, followed by the addition of 2× Laemmli buffer. Samples were boiled and resolved on a SDS–10% PAGE gel and processed as previously described (21).

The continuous protease assays were performed using fluorescence resonance energy transfer (FRET)-based substrate representing the CHIKV nsP3/4 cleavage site (34) (Fig. 4D). Briefly, a peptide substrate comprising 15 amino acids (DELRLDRAGGYIFSS) of the nsP3/4 cleavage site was commercially purchased from GeneScript, USA, which was chemically linked to the FRET pair 4-[[4-(dimethylamino)phenyl]-azo] benzoic acid (DABCYL) and 5-[(2′-aminoethyl)-amino] naphthelene-sulfonic acid (EDANS) at the amino and carboxy termini, respectively. The fluorogenic reactions were constituted in triplicates in a final volume of 200 μl (20 mM HEPES [pH 7.2] and 2 mM DTT) and 78 nM concentrations of the indicated enzymes. After the addition of the fluorogenic peptide substrates to a final concentration of 15 μM, continuous readings were recorded at 30°C on a Synergy MX microplate reader (BioTek, USA)
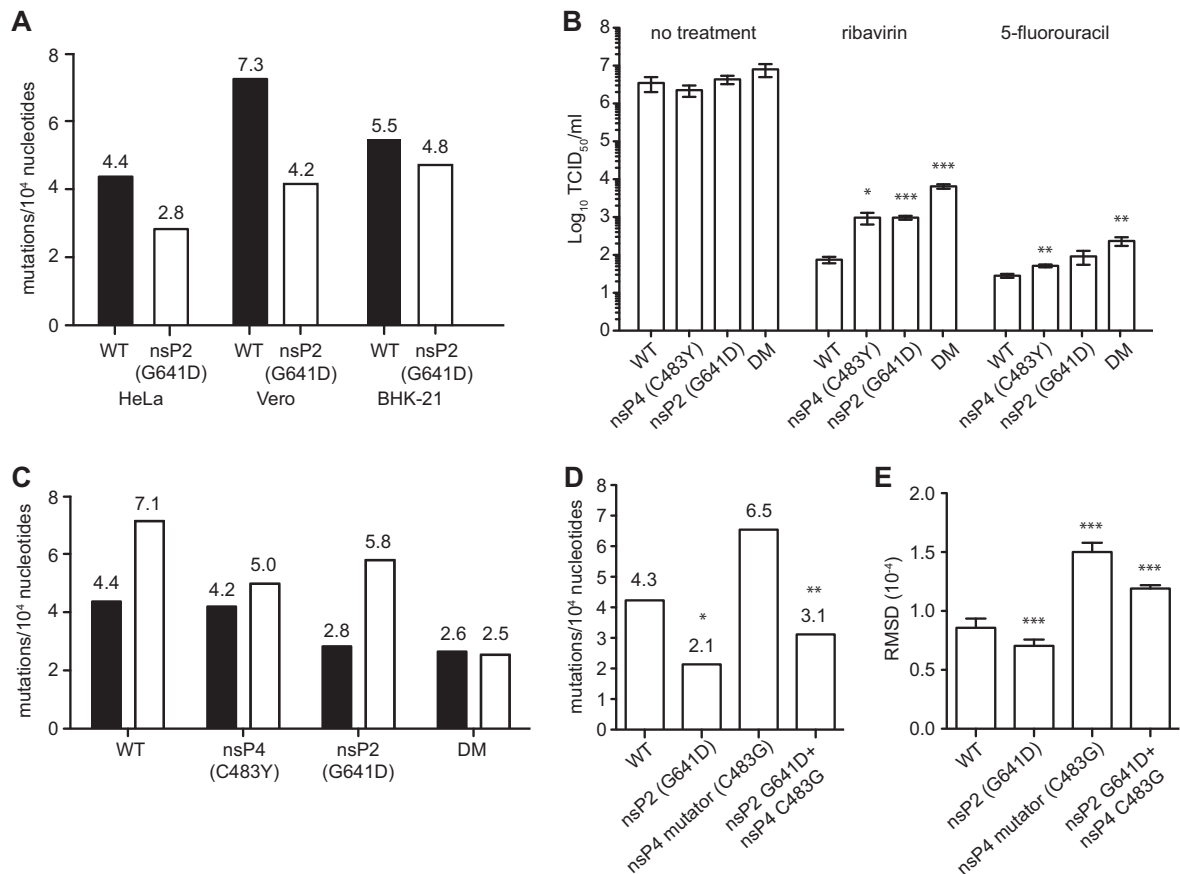
FIG 1 Chikungunya virus nsP2 regulates virus fidelity. (A) Mutation frequencies of wild-type (WT) and nsP2 (G641D) viruses in mammalian cells. (B) Virus titers of wild-type and high-fidelity variants grown in HeLa cells in the presence of the RNA mutagens ribavirin (200 μM) and 5-fluorouracil (40 μg/ml). Mean values $\pm$ the standard error of the mean (SEM) are shown ($n = 3$; *, $P < 0.05$; **, $P < 0.01$; **, $P < 0.001$ [two-way ANOVA with Bonferroni posttest]). (C) Mutation frequencies of wild type (WT) and high-fidelity variants grown in the absence (black bars) or presence (white bars) of 200 μM ribavirin. (D) Mutation frequencies by molecular cloning of wild type, high-fidelity nsp2 G641D, mutator nsp4 C483G, and the nsp2 G641D-nsp4 C483G variants (*, $P = 0.05$; **, $P = 0.0098$ [Mann-Whitney U two-tailed test]). (E) Mutation frequencies by deep sequencing as in panel D (***, $P < 0.0001$ [mean values $\pm$ the SEM, Mann-Whitney U two-tailed test]).

with an excitation wavelength of 340 nm and an emission wavelength of 490 nm at an interval of 5 min for a total period of more than 2 h. Finally, the data were normalized to a no-enzyme control and are expressed as relative fluorescence units (RFU).

In vitro **RNA helicase assays.** RNA oligonucleotide substrates with 5′ overhang for helicase assays were prepared as described previously (21). For helicase assays, a 50 pM concentration of RNA substrate was incubated with 12.5 nM purified WT nsP2 or the nsP2 G641D variant in reaction buffer containing 20 mM HEPES (pH 7.2), 2 mM DTT, and 10 mM NaCl in a final volume of 60 μl. Reaction mixtures were preincubated for 15 min at 22°C, and each reaction mixture was incubated with or without ATP-Mg^{2+} (3.5 mM, final concentration) at 30°C. Then, 5-μl aliquots were removed at the indicated time points, and the reactions were stopped and processed further as described previously (21). Images were quantified using ImageJ.

NTPase assays. NTPase assays were performed as essentially described previously by using the EnzCheck phosphate assay kit (Life Technologies) according to the manufacturer's protocol; however, the final reaction volumes were adjusted to 200 μl (33). In brief, 500 ng of purified protein was incubated in 1× reaction buffer (50 mM Tris-HCl [pH 7.5], 1 mM MgCl$_2$, 100 μM NaN$_3$) containing 200 μM 2-amino-6-mercapto-7-methylpurine riboside substrate (MESG) and 0.2 U of purine nucleoside phosphorylase in a final volume of 160 μl. After the initial incubation at 22°C for 10 min, continuous spectrophotometric measurements were carried out using an Ultro-

spec 7000 spectrophotometer (GE Healthcare) immediately after the addition of 40 μl of 1 mM nucleoside triphosphate (NTP) substrate.

In vitro **replication assay.** Portions (10 μg) of isolated membranes were added to a reaction mixture containing 1× reaction buffer (50 mM Tris-HCl [pH 8], 50 mM KCl, 3.5 mM MgCl$_2$), 10 mM DTT, 10 μg of actinomycin D/ml, 5 mM creatine phosphate, 25 μg and creatine phosphokinase/ml, 1 mM ATP, 1 mM GTP, 1 mM CTP, 50 μM UTP, 10 μCi of [α-^{32}P]UTP (Perkin-Elmer), and 1 μl of RNaseOUT (final concentration) and then incubated for the indicated time at 37°C. To examine the *in vitro* replication at low nucleotide concentrations, reactions were performed as described above but with ATP, CTP, and GTP concentrations of 10 or 100 μM. RNA was extracted with phenol-chloroform, and unincorporated nucleotides were removed using Illustra MicroSpin S200 HR columns (GE Healthcare) and separated on a 1% TAE agarose gel. Gels were dried and exposed to autoradiography film. Genomic and subgenomic RNAs were identified by size using *in vitro*-transcribed RNA standards.

Statistical tests. All experiments were performed in triplicate unless noted otherwise. Statistics, noted where applied, were performed in GraphPad Prism. P values of <0.05 were considered significant.

RESULTS

The alphavirus nonstructural protein 2 regulates genome replication fidelity. In a previous study we identified a novel mutagen-
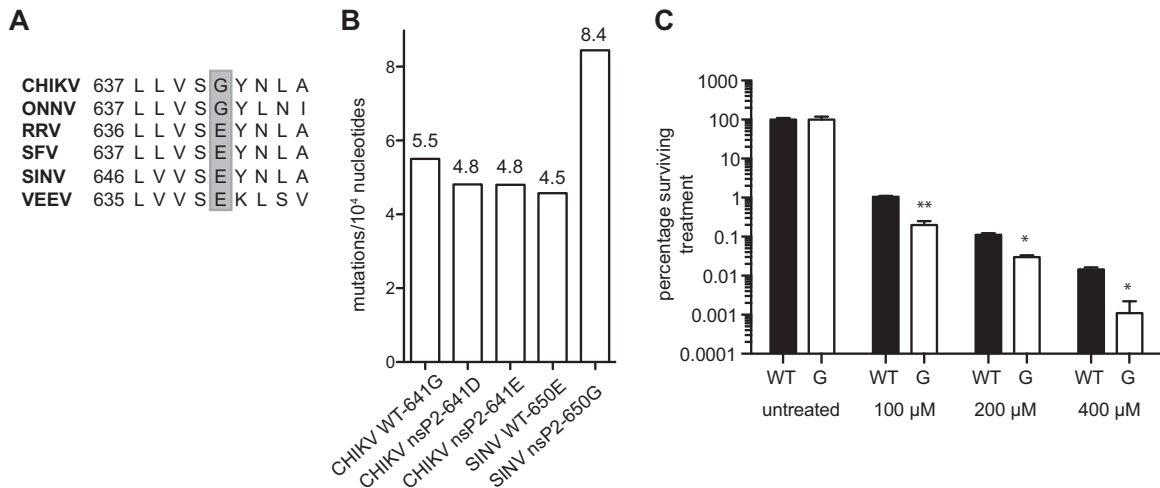
FIG 2 Regulation of virus fidelity by nsP2 is conserved among alphaviruses. (A) Amino acid alignment of the alphavirus nsp2 region. Shading indicates CHIKV position 641 and analogous residues in other alphaviruses (ONNV, O'nyong nyong virus; RRV, Ross River virus; SFV, Semliki Forest virus; VEEV, Venezuelan equine encephalitis virus). (B) Mutation frequency of Chikungunya virus wild type (WT 641G), high-fidelity 641D and 641E, and Sindbis virus wild-type 650E and low-fidelity 650G. (C) SINV wild-type and low-fidelity E650G grown in the absence (black bars) or presence (white bars) of 200 μM ribavirin. At all concentrations tested, the low-fidelity variant exhibited significant sensitivity (mean values ± the SEM, $n = 3$, two-tailed Student t test [*, $P < 0.05$; **, $P < 0.01$]).

resistant variant of CHIKV nsP2 at position 641 (G641D), suggesting that nsP2 may play an important role in maintaining replication fidelity (10). To address this possibility, we introduced this substitution into our infectious clone and measured the mutation frequencies of the resulting viral populations in multiple cell types compared to wild-type (WT) CHIKV (Fig. 1A). This variant manifested increased fidelity in every cell type, indicating that nsP2 is indeed involved in regulating CHIKV genome fidelity. Furthermore, given that both the CHIKV high-fidelity polymerase variant nsP4 (C483Y) and the novel nsP2 (G641D) variants were isolated in the same antiviral treatment, we addressed their additive roles in resistance to the RNA mutagens ribavirin and 5-fluorouracil (Fig. 1B). Both individual variants were resistant to each drug, and the combination of the two variants (DM) enhanced this further. We then addressed the mutation frequency of each virus in the absence (black bars) or presence (white bars) of ribavirin to examine the extent of mutagenesis (Fig. 1C). As expected, the wild-type population was mutagenized by the drug to the greatest degree, whereas the higher-fidelity nsP4 variant resisted mutagenesis, as previously reported (10). The nsP2 G641D single variant led to an even higher-fidelity phenotype than the nsP4 variant. Interestingly, the nsP2 and nsP4 double mutant completely resisted the mutagenic activity of ribavirin. These data suggest that these two proteins work together to regulate fidelity by nonredundant mechanisms, so the nsP2 mutation may have been selected based on the antimetabolic activities of ribavirin and 5-fluorouracil.

Given the seemingly synergistic role of nsP2 and nsP4 in regulating fidelity, we sought to determine whether the nsP2 fidelity-increasing mutation could compensate for the low-fidelity activity of a mutator variant of the nsP4 polymerase (Fig. 1D and E). To analyze this, we took advantage of a previously identified nsP4 variant C483G that has an increased mutation frequency and found that the combination of low-fidelity nsP4 with high-fidelity nsP2 yielded an intermediate mutation frequency, further suggesting these two viral components both contribute to replication fidelity.

Finally, we were interested in whether this novel function of nsP2 was conserved among the alphavirus genus. A protein alignment of the alphavirus nsP2 revealed that CHIKV and a close relative, O'nyong nyong virus (ONNV), also contain a glycine at this corresponding position, whereas other alphaviruses contain a glutamic acid (Fig. 2A). Interestingly, the increase in fidelity observed in G641D was conferred by a change to negatively charged aspartic acid, mirroring the charge of the naturally occurring glutamic acid in other alphaviruses. Therefore, we hypothesized that there is an essential requirement for a negative charge at this position for maintaining fidelity. To address this, we introduced a glutamic acid at position 641 of CHIKV and observed a decrease in mutation frequency similar to the G641D variant (Fig. 2B). In a previous study, we had observed that SINV maintained a lower basal mutation frequency (higher native fidelity) than CHIKV (11). When we changed the analogous residue in SINV from a glutamic acid to the glycine normally observed in CHIKV, the mutation frequency of SINV E650G nearly doubled (Fig. 2B). In addition, we found that SINV with the nsP2 E650G change was sensitive to ribavirin treatment (Fig. 2C), a phenotypic confirmation of reduced replication fidelity (6, 11). Taken together, these data implicate nsP2 as a key regulator of alphavirus replication fidelity, which functions together with nsP4 to maintain genomic integrity.

High-fidelity CHIKV variants have increased *in vitro* replicase activity and an increased access to nucleotides. To further study the role of these high-fidelity variants and their function in the viral life cycle, we determined one-step growth curves to address viral replication and RNA production and yet found no differences between these variants (Fig. 3A and B). This does not, however, rule out differences that may occur intracellularly or early during infection. nsP2 functions as the viral protease early during infection, cleaving the viral polyprotein in a temporal manner, which regulates multiple steps in RNA replication (35–37). To address the kinetics of polyprotein processing, we performed pulse-chase experiments on the WT and the nsP2 G641D variant, looking specifically at the cleavage of nsP1 and nsP2 dur-
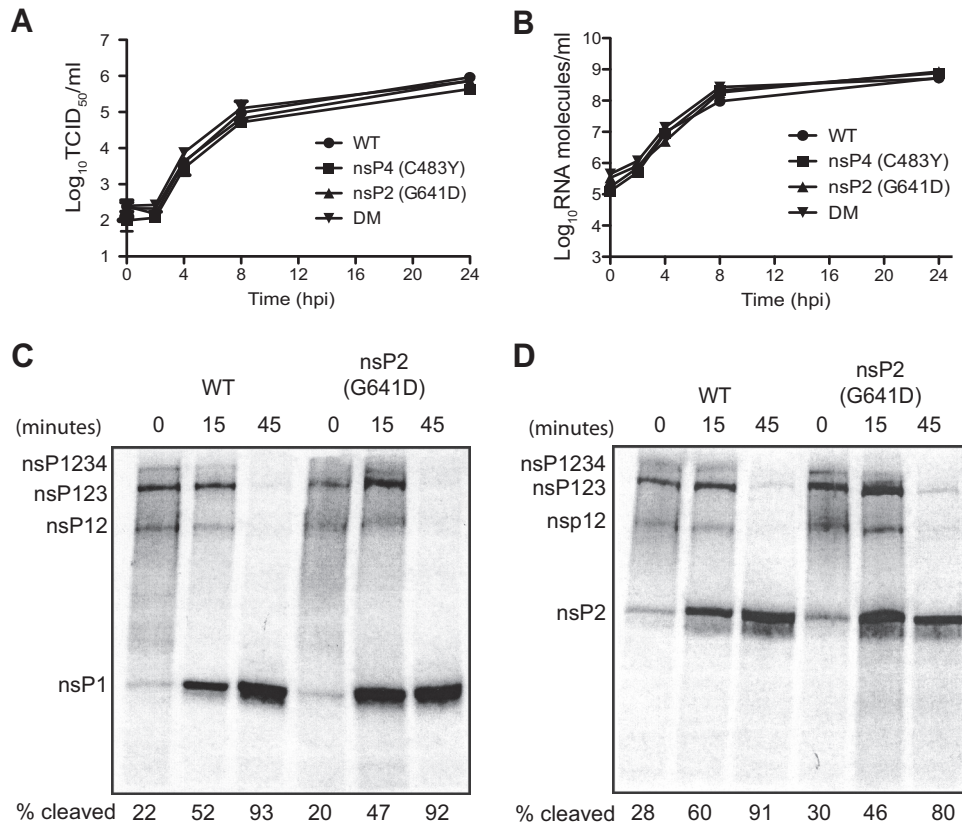
FIG 3 Chikungunya virus nsP2 high-fidelity variant does not alter viral growth or polyprotein processing. (A and B) One-step viral growth kinetics measured by infectious virion production determined by $TCID_{50}$ (A) and extracellular viral genome copies determined by qRT-PCR (B) (mean values $\pm$ the SEM, $n = 3$). (C and D) BHK-21 cells were infected at an MOI of 10 with wild type and nsP2 G641D variant. At 3 h postinfection, the cells were starved in methionine-cysteine-free medium and then pulsed with 50 μCi of [^{35}S]methionine-cysteine mixture for 15 min. The cells were collected immediately after the pulse, after 15 min, or after a 45-min chase. Synthesized nonstructural polyproteins, their processing intermediates, and mature nsPs were immunoprecipitated using either CHIKV anti-nsP1 (C) and anti-nsP2 (D) antibodies. The percent cleaved represents the fraction of fully cleaved nsP1 (C) and nsP2 (D) compared to the nsP123 polyprotein. The data for one of two reproducible independent experiments are shown.

ing the initial steps of infection, and yet no differences were observed (Fig. 3C and D). In addition to being the viral protease, nsP2 functions as a helicase and NTPase. To address these functions, we took advantage of a recently developed biochemical assay using purified nsP2 (21, 33). We purified WT nsP2 and the G641D variant and found no difference in protein purity by SDS-PAGE (Fig. 4A) or protein folding by circular dichroism spectroscopic analysis (Fig. 4B), suggesting that this mutation does not affect protein structure. Next, we addressed the *in vitro* protease activity of nsP2 by using a substrate containing the nsP2/3 cleavage site linking two larger protein fragments (21). We found no difference in nsP2 protease activity at 6 min (early events) or 1 h (late events), confirming our results from tissue culture pulse-chase analysis (Fig. 4C). Interestingly, when we used a more sensitive FRET based protease assay using the nsP3/4 cleavage site, we observed a slight increase in protease activity with the G641D variant (Fig. 4C and D). The nsP2 5A-PG variant was used as a negative control.

In addition, we addressed the helicase activity of the G641D variant, and we found no difference in helicase activity in the presence or absence of ATP and Mg^{2+} after incubation for 1 h (Fig. 5A and B). To address this further, we performed kinetic assays to look at the early events in RNA unwinding (Fig. 5C and

D). Here, we found the G641D variant to present impaired helicase function early in the boost phase of unwinding and to plateau at a lower level compared to wild-type nsP2. Finally, we looked at the relative NTPase activity of these purified proteins and found that the nsP2 high-fidelity variant G641D exhibited increased NTPase activity for all NTP substrates *in vitro* (Fig. 5E and F). The 5A-PG variant was used a negative control.

These data suggest that nsP2 G641D may play a role in the replication complex's ability to hydrolyze nucleotides; however, since the other nonstructural proteins have not yet been successfully biochemically purified and tested *in vitro*, we could not test this further. As an alternative approach, we isolated functional replication complexes by differential centrifugation from infected cells to determine the kinetics of *in vitro* RNA synthesis and biochemical characteristics of these complexes, which contained equal amounts of all viral proteins (Fig. 6A). We found that high-fidelity nsP4 variant C483Y and the double mutant had more rapid kinetics compared to wild-type, whereas the nsP2 variant G641D had an intermediate phenotype (Fig. 6B and C). These increased replication kinetics and NTPase activities of nsP2 lead us to hypothesize that the high-fidelity variants are better able to access or utilize nucleotide pools, increasing the overall rate of polymerization. Because ribavirin is known to deplete GTP pools,
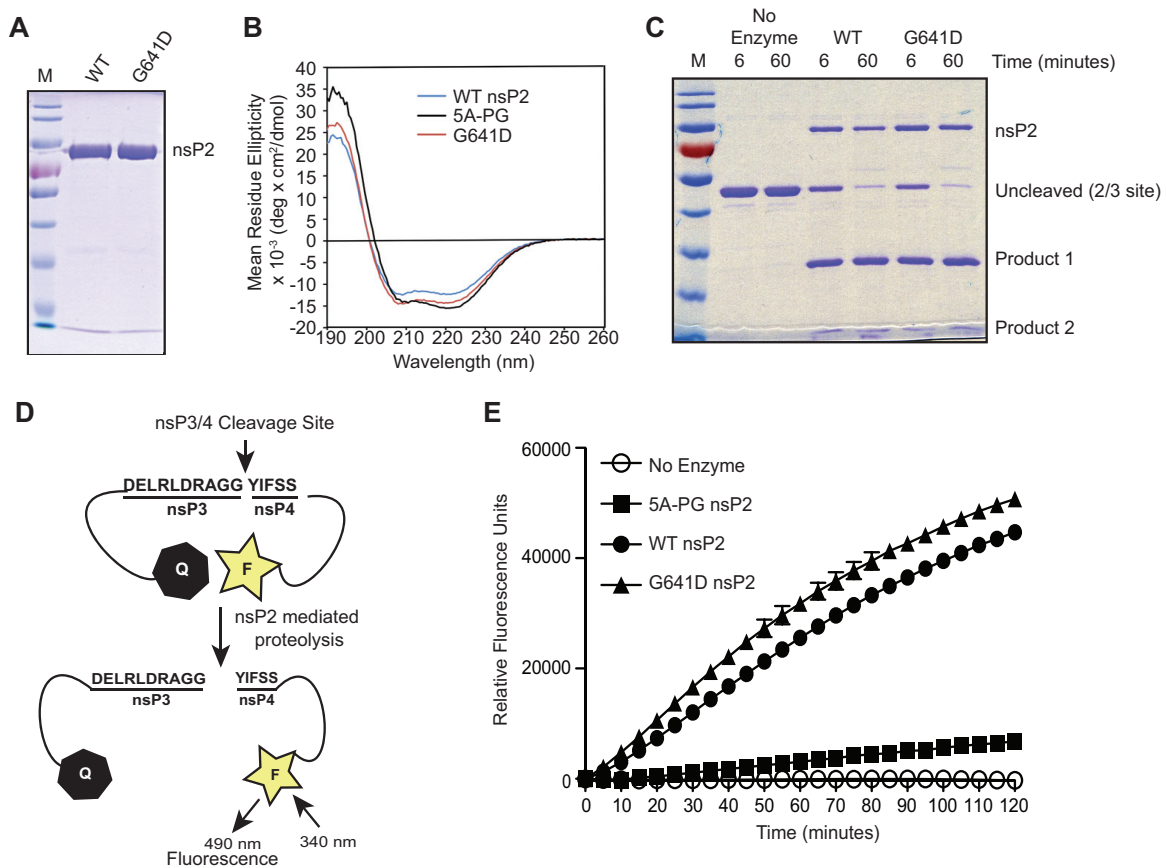
FIG 4 Purified CHIKV nsP2 G641D increases protease activity *in vitro*. (A) SDS-PAGE gel of purified wild-type and nsP2 G641D proteins. (B) Circular dichroism spectra of purified WT, an unrelated nsP2 mutant as a control, and nsP2 G641D. (C) Coomassie blue-stained protein gel showing the ability of purified nsP2 to cleave the nsP2/3 cleavage sites using an *in vitro* protease assay. Substrates were incubated for 6 min or 1 h with purified proteins. UT, no enzyme control. (D) Schematic of FRET-based protease assay. (E) Quantification of FRET-based protease assay using wild-type nsP2, nsP2 G641D, and nsP2 5A-PG as a negative control (mean values ± the SEM, *n* = 2).

we hypothesized that increased polymerization in limiting NTP conditions could lead to the resistance we observe in the presence of ribavirin. To study this, we incubated isolated replication complexes in low nucleotide concentrations and addressed the amount of RNA synthesized *in vitro* (Fig. 6D and E). We found that whereas wild-type replication complex activity was reduced roughly 2-fold when nucleotides were limiting, the activity of all three high-fidelity variants was reduced to a greater extent under these conditions (Fig. 6E). Taken together, these data suggest that high-fidelity variants of nsP4 and nsP2 may reduce their replicase activity to become more selective to nucleotide pools and replicate more efficiently even at low nucleotide concentrations.

CHIKV high-fidelity replicase variants confer resistance to inhibitors of nucleoside biosynthesis. The nsP2 and nsP4 variants were selected in the presence of ribavirin, an RNA mutagen that is also a purine biosynthesis inhibitor. Therefore, we hypothesized that the antiviral effects of ribavirin on viral growth should be at least partially complemented by the addition of exogenous nucleosides. Indeed, we found that the viral growth of the high-fidelity variants increased with low concentrations of guanosine, and at high concentrations all viruses, including wild type, were rescued (Fig. 7A). As a control, we added uridine, which was unable to rescue viral growth to the extent of guanosine. These data

reinforce previous studies that the antiviral effect of ribavirin contributes at two levels: at the primary level of nucleotide depletion and at the secondary level as a RNA mutagen.

The results obtained by ribavirin treatment in conjunction with rescue by addition of nucleotides suggest that the nsP2 variant may have an advantage in nucleotide-depleted cells, similar to what we observed by measuring of mutation frequencies in the presence of ribavirin, and in our biochemical assays. We thus sought to determine whether these variants were resistant to other nucleotide-depleting compounds, using mycophenolic acid and brequinar, which are not nucleoside analogues. Mycophenolic acid inhibits IMPDH, acting analogously to ribavirin to deplete GTP pools. In contrast, brequinar is a compound that acts by inhibiting dihydroorotate dehydrogenase, a key enzyme in pyrimidine synthesis, depleting both CTP and TTP (38, 39). By treating cells during viral infection with each compound, we found that the high-fidelity nsP2 variant and double mutant were more resistant to both nucleotide-depleting compounds (Fig. 7B and C), similar to what we observed with ribavirin treatment. Interestingly, the nsP4 high-fidelity variant was not resistant to pyrimidine depletion and the addition of this variant to nsP2 G641D did not further enhance the resistance of the single nsP2 mutation, suggesting that nsP2 and nsP4 may function independently under these condi-
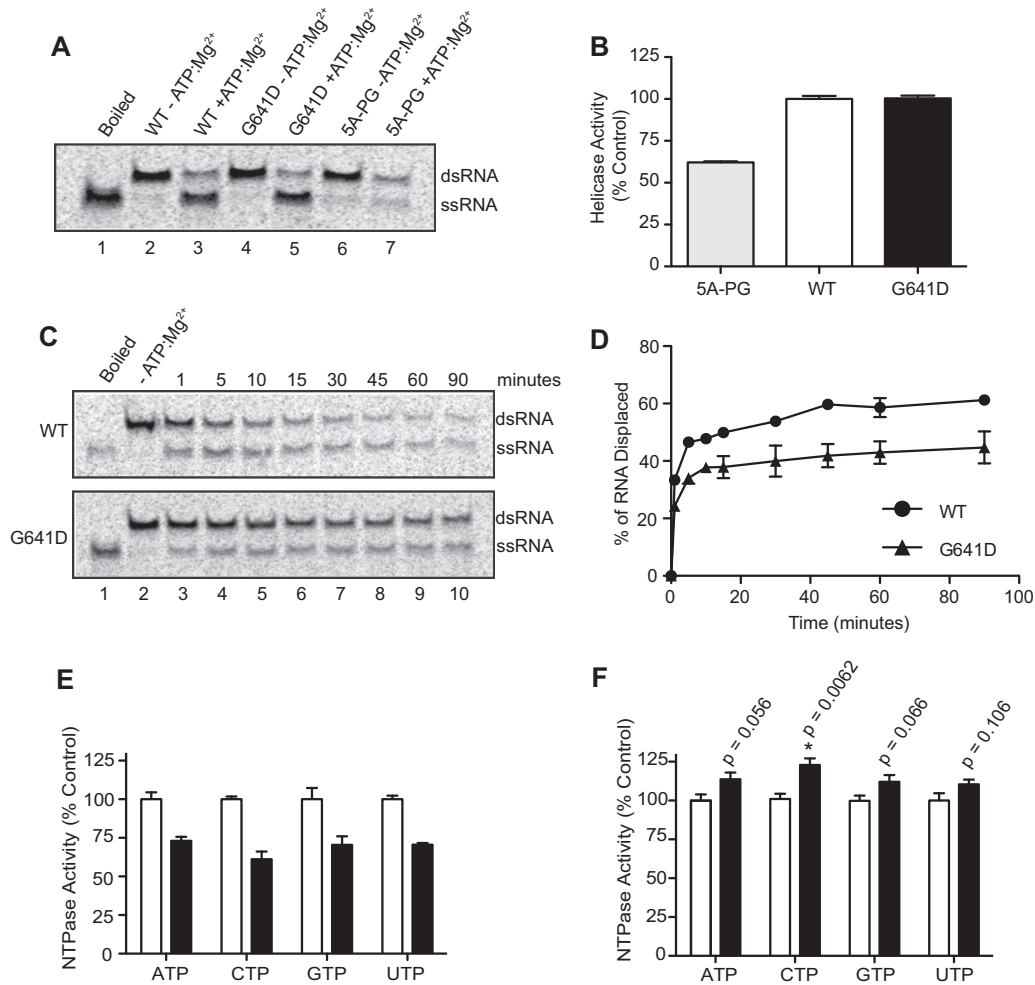
FIG 5 Purified CHIKV nsP2 G641D has reduced helicase activity and increased NTPase activity *in vitro*. (A) One-hour endpoint helicase assay. Purified proteins were incubated with dsRNA subtract for 1 h in the presence or absence of ATP and Mg^{2+}. nsP2 5A-PG was used as a negative control (lanes 6 and 7). (B) Quantification of the data in panel A. (C) Kinetic analysis of wild-type nsP2 and G641D helicase activity. Purified proteins and dsRNA substrates were incubated at 30°C, and aliquots were removed at the indicated time points. (D) Quantification of kinetic analysis in panel C. (E) NTPase activity of wild-type nsP2 (white bars) and nsP2 5A-PG (black bars) as a negative control. (F) NTPase activity of wild-type nsP2 (white bars) and nsP2 G641D (black bars). Mean values ± the SEM are shown ($n = 5$, Student t test [*, $P < 0.05$]).

tions. Furthermore, viral growth was restored with the addition of relevant exogenous nucleosides, whereas the addition of irrelevant nucleosides was not effective for restoring viral growth, confirming that nucleotide depletion was leading to viral attenuation. Taken together, these data show that high-fidelity variants are more resistant to nucleotide-depleting conditions and that the selection of these variants in the presence of these compounds suggests that RNA viruses can regulate their fidelity to compensate for such intracellular changes.

DISCUSSION

The vast majority of work focusing on RNA virus replication fidelity has highlighted the essential role of the RdRp in maintaining genomic integrity. Past works were largely facilitated by selecting for viruses resistant to RNA mutagens, thus yielding a polymerase that is more resistant to nucleoside analogue misincorporation. In a previous study, we passaged CHIKV in the presence of mutagens in order to identify a high-fidelity alphavirus polymerase. Unexpectedly, in the process we uncovered a variant of the helicase/

protease (nsp2 G641D) in addition to a high-fidelity polymerase variant (C483Y) (10). Here, we explored the role of this variant and nsP2 in resistance to RNA mutagens, fluctuations in nucleotide pools, and fidelity. We found that this single substitution in nsP2 led to resistance to several RNA mutagens, as well as nucleotide synthesis inhibitors. In addition, this variant increased the fidelity of CHIKV in multiple cell types, providing a novel role for the nsP2 protein in the viral life cycle and demonstrating that other nonstructural proteins play important roles in RNA replication fidelity aside from the polymerase itself. One possible explanation for these changes in fidelity could be due to changes in physical interactions between nsP2 and nsP4, particularly since these mutations were always found on the same genomes in the original screen for resistance to ribavirin and 5-fluorouracil. Nonetheless, this does not rule out the possibility of differences in physical interactions or binding affinities with other viral nonstructural proteins in the replication complex. Interestingly, mutations in the nsP1 of SINV conferring ribavirin resistance have
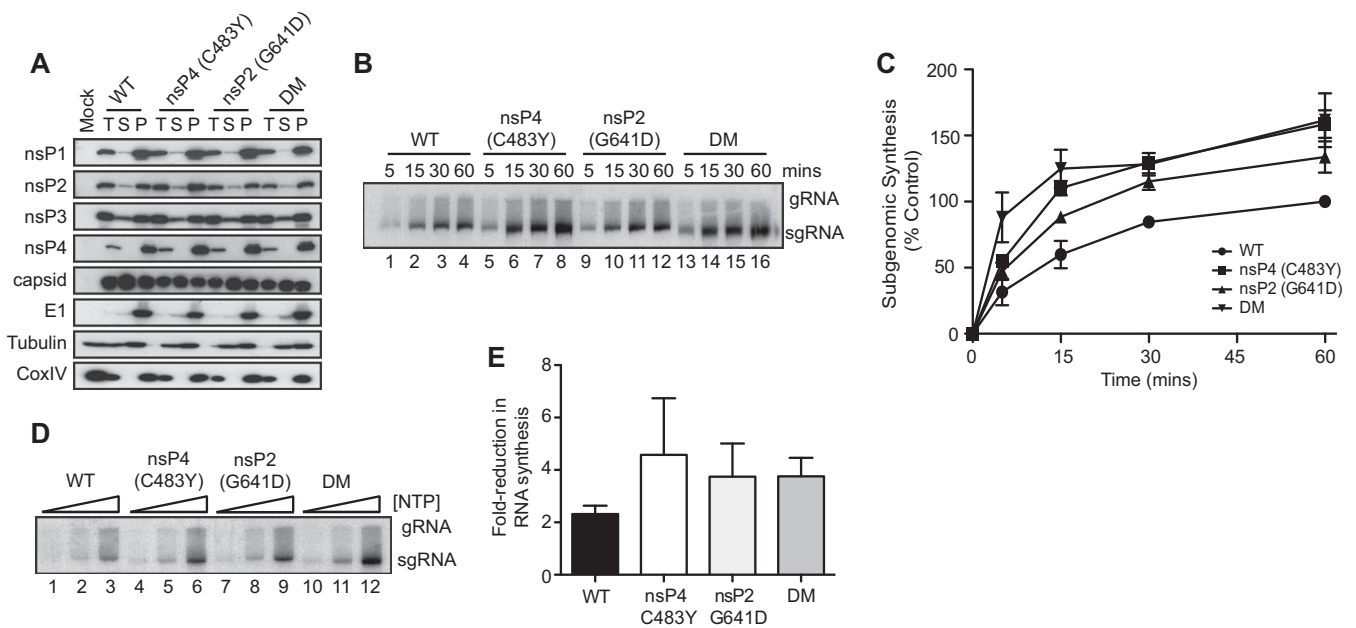
FIG 6 CHIKV high-fidelity replication complexes have increased *in vitro* RNA polymerase activity and are less sensitive to nucleotide depletion. (A) Immunoblot showing subcellular localizations of viral proteins (*n* = 2). T, total extract; S, soluble fraction; P, pellet. (B) Autoradiogram of time course of *in vitro* replication for CHIKV wild type, nsp4 C483Y, nsp2 G641D, and DM. (C) Quantification subgenomic RNA synthesis from *in vitro* replication assay in panel B (mean values ± the SEM, *n* = 3). (D) *In vitro* replication assay in the presence of 10, 100, and 1,000 μM NTP. Membranes were incubated for 3 h at 37°C. (E) Quantification of subgenomic synthesis in nucleotide depleted conditions in panel D (Student *t* test, *n* = 3 [*, *P* < 0.05; **, *P* < 0.01]).

been described (40). It would be interesting to test whether these mutations in nsp1 also alter viral replication fidelity by mechanisms similar to what we describe for nsP2 G641D. Currently, nonpolymerase fidelity determinants for RNA viruses have only been described in coronaviruses, which are unique in having a proofreading RNase (ExoN) (41). Manipulating ExoN or its viral cofactor nsp10 yields variants with altered fidelity (42). Helicase-like accessory proteins, on the other hand, are common across many RNA viruses and may be a more general mechanism of complementing RNA polymerase fidelity.

Not only did the nsP2 variant confer resistance to ribavirin and 5-fluorouracil, but the addition of the nsP4 high-fidelity polymerase variant further increased resistance to these mutagens, supporting that these two proteins are functionally linked to modulate replication fidelity by complementary mechanisms. This was highlighted by the additive increase in fidelity of the double mutant containing a high-fidelity polymerase, and the restoration of wild-type-like mutation frequencies in the double mutant containing a low-fidelity polymerase. In fact, the nsP2-nsP4 high-fidelity double mutant showed no sign of mutagenesis in the presence of ribavirin. These results suggest that these high-fidelity replication complexes are selectively incorporating nucleotides in such a way that ribavirin cannot enter the replication complex or be incorporated into the growing RNA strand possibly due to selective steric hindrance or increased affinity to intracellular nucleotides. Importantly, our data suggest that the mutagenic effects of base analogs resulting from misincorporation is potentiated under conditions of nucleotide depletion, when natural bases may not be available or accessible. This finding is of importance to optimize the design of future nucleoside analogues, to either more closely resemble natural nucleotides and/or increase their effects on natural nucleotide pools.

In addition to a role of nsP2 in regulating CHIKV replication fidelity, we were interested in whether these characteristics were shared between other alphaviruses. In previous studies, we observed that the mutation frequency of SINV was naturally lower than that of CHIKV. The amino acid sequence alignment of this region between several alphaviruses indicated that, with the exception of ONNV, other alphaviruses contained a negatively charged glutamic acid instead of a glycine (Fig. 2A). This negatively charged residue is similar to the aspartic acid that was selected in ribavirin treatment, suggesting that having a negative charge at this position plays an important role in maintaining replication fidelity. Indeed, when we changed the G641D variant from an aspartic to a glutamic acid to mimic the other alphaviruses we obtained the same high-fidelity phenotype. Furthermore, when we changed the glutamic acid of SINV to a glycine, we increased the mutation frequency of SINV, appreciably further confirming the role of this residue and nsP2 protein in determining replication fidelity of this virus genus. Importantly, if manipulating this residue is a genus-wide determinant of fidelity, mutator variants for other alphaviruses could be easily obtained. Mutator strains, which are known to result in attenuation *in vivo* (6, 11, 43), could provide novel therapeutic vaccine strategies.

To understand the mechanisms by which the nsP2 high-fidelity variant was changing mutation frequency, we used a biochemical system that has been used to study a variety of aspects of nsP2 biology (21, 33). Using this system, we identified differences in the relative helicase and NTPase activity of the 641D variant. We observed a trend in increased NTPase activity for all nucleotides but a reduction in helicase activity *in vitro*. Overall increases in NTPase activity by G641D combined with the WT polymerase of (relatively) lower fidelity may provide support as to why the nsP2 641D replication complex is most sensitive to ribavirin misincor-
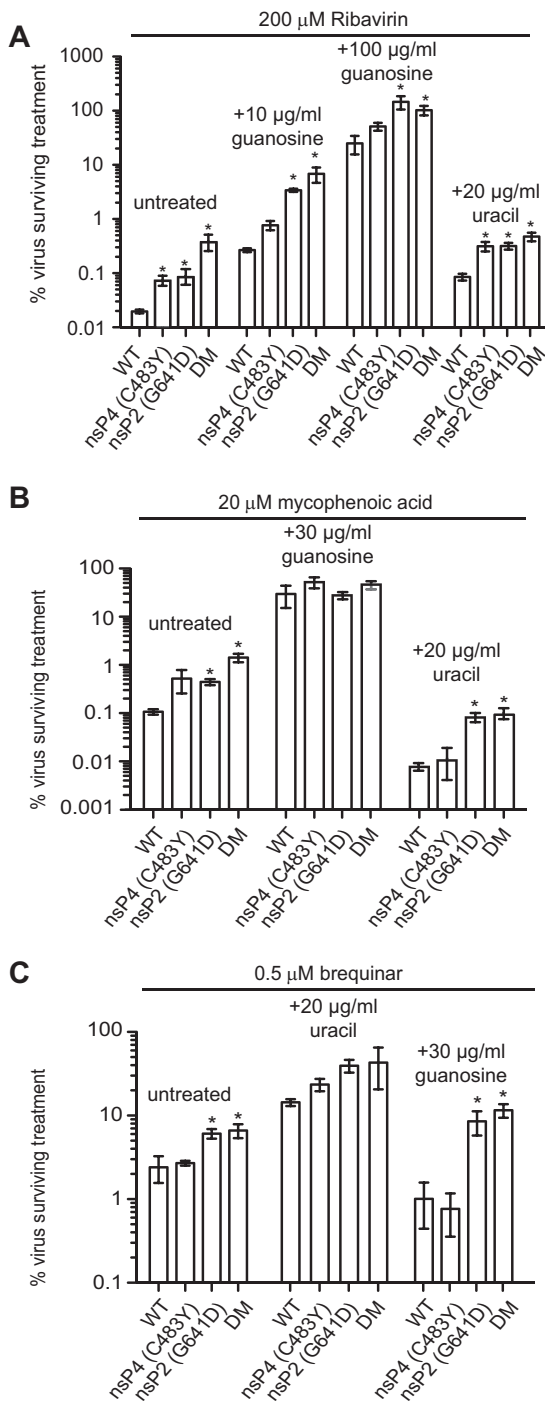
FIG 7 CHIKV high-fidelity variants are resistant to nucleotide biosynthesis inhibitors and can be rescued with exogenous nucleotides. (A) Viruses were grown in the presence of 200 µM ribavirin and either left untreated (no exogenous nucleosides) or complemented with 10 or 100 µg of guanosine/ml or 20 µg of uracil/ml. (B) Viruses were grown in the presence of mycophenolic acid and either left untreated (no exogenous nucleosides) or complemented with 30 µg of guanosine/ml or 20 µg of uracil/ml. (C) Viruses were grown in the presence of brequinar and either left untreated (no exogenous nucleosides) or complemented with 20 µg of uracil/ml or 30 µg of guanosine/ml. For all panels, mean values ± the SEM are shown ($n = 3$; *, $P < 0.05$ [two-way analysis of variance with Bonferroni posttest]).

poration among the high-fidelity viruses (compare Fig. 1C, C483Y and G641D), whereas a combination of nsP2 641D and 483Y yields a complex that is largely unable to acquire ribavirin. In addition, slower helicase activity may provide a basis for selective nucleotide incorporation. However, it should be noted that although these results are intriguing and this system is robust and sufficient for studying purified nsP2, it is lacking all other components of the replication complex, which have yet to be successfully expressed *in vitro*. These missing components will more then likely influence many aspects of nsP2 biology, and thus these *in vitro* results, while informative, should be interpreted with this in mind.

Given the lack of a biochemical system to examine nsP4 in isolation, we addressed the replication activity of isolated active replication complexes from infected cells. In contrast to previous work showing reduced replication rate can increase selectivity and fidelity, we found that high-fidelity replication complexes had increased kinetics compared to the wild type. An explanation for this discrepancy could be the ability of the replication complex to receive and process nucleotides at an increased rate (due to changes in the structural arrangement of the replication complex) and thus have a greater ability to access and process the necessary components for RNA synthesis, while still possessing a high-fidelity state. Nonetheless, these results, which are in contradiction to the observations that a polymerase that makes fewer errors generally manifests a slower polymerization rate (44). It is also possible that such contrasting results are caused by technical differences in the assays used, since correct nucleotide incorporation assays use synthetic substrates and purified polymerases in isolation, in abbreviated nucleotide incorporation cycles. Regardless, it is likely that replicase function and fidelity is not only regulated at nucleotide access but at multiple levels, including RNA structure, replicase protein-protein interactions and processivity, RNA-protein interactions, and host components, all areas that need to be addressed to fully understand replicase fidelity.

In addition to increased kinetics at more optimal conditions, we addressed the activity of high-fidelity replication complexes in low nucleotide conditions. We found that when nucleotide levels were reduced 10-fold, the high-fidelity replication complex activity was reduced to a greater extent than wild type and yet still was capable of synthesizing more RNA and in turn overcoming low nucleotide levels. We speculate that these variants have adopted finely calibrated replication complexes that allow for greater access to incoming nucleotides (or other necessary components) or higher processivity of nucleotides once they are encountered.

On the basis of these *in vitro* and biochemical studies and given the pleiotropic effects of ribavirin, we then addressed the resistance of the high-fidelity variants to compounds that deplete intracellular nucleotide levels and yet are not reported to be nucleoside analogues, such as mycophenolic acid and brequinar. We found that all of the high-fidelity variants resisted the antiviral effects of mycophenolic acid better than WT CHIKV, whereas only the nsP2 G641D variant conferred resistance to brequinar. In addition, viral growth could be rescued with the addition of relevant exogenous nucleosides. These results in tissue culture support our *in vitro* and biochemical results that high-fidelity variants are able to function better in the presence of low levels of nucleotide. In particular, the resistance of nsP2 G641D and not nsP4 C483Y to brequinar and pyrimidine depletion may explain the enhanced NTPase activity of the G641D variant to the pyrimidines

CTP and UTP. Furthermore, since we were able to completely restore virus titers after drug treatment with the addition of exogenous nucleotides, our data do suggest that these compounds may be more effective RNA mutagens only when natural nucleotide pools are concomitantly depleted, an observation that is supported by the ability to complement the mutagenic effect of ribavirin and mycophenolic acid with the addition of relevant nucleosides (45).

In summary, we show the essential role and novel function of nsP2 in maintaining alphavirus replication complex fidelity. Furthermore, our evidence supports the long-standing hypothesis for a concerted and dynamic interaction between viral helicases and polymerases to orchestrate replication fidelity (46). These studies highlight the mechanisms by which RNA viruses respond to their intracellular environments to replication fidelity in low nucleotide concentrations. Given that many nucleoside analogs and RNA mutagens are already used or being considered in clinical settings, understanding the mechanisms by which they increase mutation rates will facilitate their use as broad-spectrum antivirals.

REFERENCES

1. Zeng J, Wang H, Xie X, Li C, Zhou G, Yang D, Yu L. 2014. Ribavirin-resistant variants of foot-and-mouth disease virus: the effect of restricted quasispecies diversity on viral virulence. J Virol 159:2641–2650. http://dx.doi.org/10.1007/s00705-014-2126-z.

2. Arias A, Arnold JJ, Sierra M, Smidansky ED, Domingo E, Cameron CE. 2008. Determinants of RNA-dependent RNA polymerase (in)fidelity revealed by kinetic analysis of the polymerase encoded by a foot-and-mouth disease virus mutant with reduced sensitivity to ribavirin. J Virol 82:12346–12355. http://dx.doi.org/10.1128/JVI.01297-08.

3. Pfeiffer JK, Kirkegaard K. 2003. A single mutation in poliovirus RNA-dependent RNA polymerase confers resistance to mutagenic nucleotide analogs via increased fidelity. Proc Natl Acad Sci U S A 100:7289–7294. http://dx.doi.org/10.1073/pnas.1232294100.

4. Vignuzzi M, Stone JK, Arnold JJ, Cameron CE, Andino R. 2005. Quasispecies diversity determines pathogenesis through cooperative interactions in a viral population. Nature 439:344–348.

5. Levi LI, Gnädig NF, Beaucourt S, McPherson MJ, Baron B, Arnold JJ, Vignuzzi M. 2010. Fidelity variants of RNA-dependent RNA polymerases uncover an indirect, mutagenic activity of amiloride compounds. PLoS Pathog 6:e1001163. http://dx.doi.org/10.1371/journal.ppat.1001163.

6. Gnädig NF, Beaucourt S, Campagnola G, Bordería AV, Sanz-Ramos M, Gong P, Blanc H, Peersen OB, Vignuzzi M. 2012. Coxsackievirus B3 mutator strains are attenuated in vivo. Proc Natl Acad Sci U S A 109:E2294–E2303. http://dx.doi.org/10.1073/pnas.1204022109.

7. Cheung PPH, Watson SJ, Choy K-T, Fun Sia S, Wong DDY, Poon LLM, Kellam P, Guan Y, Malik Peiris JS, Yen H-L. 2014. Generation and characterization of influenza A viruses with altered polymerase fidelity. Nat Commun 5:4794. http://dx.doi.org/10.1038/ncomms5794.

8. Sadeghipour S, Bek EJ, McMinn PC. 2013. Ribavirin-resistant mutants of human enterovirus 71 express a high replication fidelity phenotype during growth in cell culture. J Virol 87:1759–1769. http://dx.doi.org/10.1128/JVI.02139-12.

9. Meng T, Kwang J. 2014. Attenuation of human enterovirus 71 high-replication-fidelity variants in AG129 mice. J Virol 88:5803–5815. http://dx.doi.org/10.1128/JVI.00289-14.

10. Coffey LL, Beeharry Y, Bordería AV, Blanc H, Vignuzzi M. 2011.

11. Arbovirus high fidelity variant loses fitness in mosquitoes and mice. Proc Natl Acad Sci U S A 108:16038–16043. http://dx.doi.org/10.1073/pnas.1111650108.

11. Rozen-Gagnon K, Stapleford KA, Mongelli V, Blanc H, Failloux A-B, Saleh M-C, Vignuzzi M. 2014. Alphavirus mutator variants present host-specific defects and attenuation in mammalian and insect models. PLoS Pathog 10:e1003877. http://dx.doi.org/10.1371/journal.ppat.1003877.

12. Crotty S, Andino R. 2002. Implications of high RNA virus mutation rates: lethal mutagenesis and the antiviral drug ribavirin. Microbes Infect 4:1301–1307. http://dx.doi.org/10.1016/S1286-4579(02)00008-4.

13. Beaucourt S, Vignuzzi M. 2014. Ribavirin: a drug active against many viruses with multiple effects on virus replication and propagation: molecular basis of ribavirin resistance. Curr Opin Virol 8:10–15. http://dx.doi.org/10.1016/j.coviro.2014.04.011.

14. Wray SK, Gilbert BE, Knight V. 1985. Effect of ribavirin triphosphate on primer generation and elongation during influenza virus transcription in vitro. Antivir Res 5:39–48. http://dx.doi.org/10.1016/0166-3542(85)90013-0.

15. Leyssen P, Balzarini J, De Clercq E, Neyts J. 2005. The predominant mechanism by which ribavirin exerts its antiviral activity in vitro against flaviviruses and paramyxoviruses is mediated by inhibition of IMP dehydrogenase. J Virol 79:1943–1947. http://dx.doi.org/10.1128/JVI.79.3.1943-1947.2005.

16. Longley DB, Harkin DP, Johnston PG. 2003. 5-Fluorouracil: mechanisms of action and clinical strategies. Nat Rev Cancer 3:330–338. http://dx.doi.org/10.1038/nrc1074.

17. Solignat M, Gay B, Higgs S, Briant L, Devaux C. 2009. Replication cycle of Chikungunya: a re-emerging arbovirus. Virology 393:183–197. http://dx.doi.org/10.1016/j.virol.2009.07.024.

18. Ahola T, Kääriäinen L. 1995. Reaction in alphavirus mRNA capping: formation of a covalent complex of nonstructural protein nsP1 with 7-methyl-GMP. Proc Natl Acad Sci U S A 92:507–511. http://dx.doi.org/10.1073/pnas.92.2.507.

19. Karpe YA, Aher PP, Lole KS. 2011. NTPase and 5'-RNA triphosphatase activities of Chikungunya virus nsP2 protein. PLoS One 6:e22336. http://dx.doi.org/10.1371/journal.pone.0022336.

20. Bourai M, Lucas-Hourani M, Gad HH, Drosten C, Jacob Y, Tafforeau L, Cassonnet P, Jones LM, Judith D, Couderc T, Lecuit M, Andre P, Kummerer BM, Lotteau V, Despres P, Tangy F, Vidalain PO. 2012. Mapping of Chikungunya virus interactions with host proteins identified nsP2 as a highly connected viral component. J Virol 86:3121–3134. http://dx.doi.org/10.1128/JVI.06390-11.

21. Utt A, Das PK, Varjak M, Lulla V, Lulla A, Merits A. 2015. Mutations conferring a noncytotoxic phenotype on Chikungunya virus replicons compromise enzymatic properties of nonstructural protein 2. J Virol 89:3145–3162. http://dx.doi.org/10.1128/JVI.03213-14.

22. Fros JJ, van der Maten E, Vlak JM, Pijlman GP. 2013. The C-terminal domain of Chikungunya virus nsP2 independently governs viral RNA replication, cytopathicity, and inhibition of interferon signaling. J Virol 87:10394–10400. http://dx.doi.org/10.1128/JVI.00884-13.

23. Fros JJ, Fros JJ, Major LD, Major LD, Scholte FEM, Scholte FEM, Gardner J, Gardner J, van Hemert MJ, van Hemert MJ, Suhrbier A, Suhrbier A, Pijlman GP, Pijlman GP. 2015. Chikungunya virus nonstructural protein 2-mediated host shut-off disables the unfolded protein response. J Gen Virol 96:580–589. http://dx.doi.org/10.1099/vir.0.071845-0.

24. Fros JJ, Liu WJ, Prow NA, Geertsema C, Ligtenberg M, Vanlandingham DL, Schnettler E, Vlak JM, Suhrbier A, Khromykh AA, Pijlman GP. 2010. Chikungunya virus nonstructural protein 2 inhibits type I/II interferon-stimulated JAK-STAT signaling. J Virol 84:10877–10887. http://dx.doi.org/10.1128/JVI.00949-10.

25. Rathore APS, Haystead T, Das PK, Merits A, Ng M-L, Vasudevan SG. 2014. Chikungunya virus nsP3 and nsP4 interacts with HSP-90 to promote virus replication: HSP-90 inhibitors reduce CHIKV infection and inflammation in vivo. Antivir Res 103:7–16. http://dx.doi.org/10.1016/j.antiviral.2013.12.010.

26. McKnight KL, Simpson DA, Lin SC, Knott TA, Polo JM, Pence DF, Johannsen DB, Heidner HW, Davis NL, Johnston RE. 1996. Deduced consensus sequence of Sindbis virus strain AR339: mutations contained in laboratory strains which affect cell culture and in vivo phenotypes. J Virol 70:1981–1989.

27. Beaucourt S, Borderia AV, Coffey LL, Gnadig NF, Sanz-Ramos M, Beeharry Y, Vignuzzi M. 2011. Isolation of fidelity variants of RNA

viruses and characterization of virus mutation frequency. J Vis Exp **52:** pii2953. http://dx.doi.org/10.3791/2953.

28. **Li H, Durbin R.** 2009. Fast and accurate short read alignment with Burrows-Wheeler transform. Bioinformatics **25:**1754–1760. http://dx.doi .org/10.1093/bioinformatics/btp324.

29. **Li H, Handsaker B, Wysoker A, Fennell T, Ruan J, Homer N, Marth G, Abecasis G, Durbin R, Subgroup 1GPDP.** 2009. The sequence alignment/map format and SAMtools. Bioinformatics **25:**2078–2079. http://dx .doi.org/10.1093/bioinformatics/btp352.

30. **Isakov O, Bordería AV, Golan D, Hamenahem A, Celniker G, Yoffe L, Blanc H, Vignuzzi M, Shomron N.** 2015. Deep sequencing analysis of viral infection and evolution allows rapid and detailed characterization of viral mutant spectrum. Bioinformatics **31:**2141–2150. http://dx.doi.org /10.1093/bioinformatics/btv101.

31. **Lanciotti RS, Kosoy OL, Laven JJ, Panella AJ, Velez JO, Lambert AJ, Campbell GL.** 2007. Chikungunya virus in US travelers returning from India, 2006. Emerg Infect Dis **13:**764–767. http://dx.doi.org/10.3201 /eid1305.070015.

32. **Coffey LL, Vignuzzi M.** 2011. Host alternation of Chikungunya virus increases fitness while restricting population diversity and adaptability to novel selective pressures. J Virol **85:**1025–1035. http://dx.doi.org/10.1128 /JVI.01918-10.

33. **Das PK, Merits A, Lulla A.** 2014. Functional cross-talk between distant domains of Chikungunya virus non-structural protein 2 is decisive for its RNA-modulating activity. J Biol Chem **289:**5635–5653. http://dx.doi.org /10.1074/jbc.M113.503433.

34. **Matayoshi ED, Wang GT, Krafft GA, Erickson J.** 1990. Novel fluorogenic substrates for assaying retroviral proteases by resonance energy transfer. Science **247:**954–958. http://dx.doi.org/10.1126/science .2106161.

35. **Sawicki DL, Perri S, Polo JM, Sawicki SG.** 2006. Role for nsP2 proteins in the cessation of alphavirus minus-strand synthesis by host cells. J Virol **80:**360–371. http://dx.doi.org/10.1128/JVI.80.1.360-371.2006.

36. **Russo AT, Malmstrom RD, White MA, Watowich SJ.** 2010. Structural basis for substrate specificity of alphavirus nsP2 proteases. J Mol Graphics Model **29:**46–53. http://dx.doi.org/10.1016/j.jmgm.2010.04.005.

37. **Russo AT, White MA, Watowich SJ.** 2006. The crystal structure of the Venezuelan equine encephalitis alphavirus nsP2 protease. Structure **14:** 1449–1458. http://dx.doi.org/10.1016/j.str.2006.07.010.

38. **Lucas-Hourani M, Dauzonne D, Jorda P, Cousin G, Lupan A, Helynck O, Caignard G, Janvier G, André-Leroux G, Khiar S, Escriou N, Després P, Jacob Y, Munier-Lehmann H, Tangy F, Vidalain P-O.** 2013. Inhibition of pyrimidine biosynthesis pathway suppresses viral growth through innate immunity. PLoS Pathog **9:**e1003678. http://dx.doi.org/10.1371 /journal.ppat.1003678.

39. **Cholewiński G, Iwaszkiewicz-Grzes D, Prejs M, Głowacka A, Dzierzbicka K.** 2015. Synthesis of the inosine 5∅-monophosphate dehydrogenase (IMPDH) inhibitors. J Enzyme Inhibition Med Chem **30:**550–563. http://dx.doi.org/10.3109/14756366.2014.951349.

40. **Scheidel LM, Durbin RK, Stollar V.** 1987. Sindbis virus mutants resistant to mycophenolic acid and ribavirin. Virology **158:**1–7. http://dx.doi.org /10.1016/0042-6822(87)90230-3.

41. **Smith EC, Blanc H, Vignuzzi M, Denison MR.** 2013. Coronaviruses lacking exoribonuclease activity are susceptible to lethal mutagenesis: evidence for proofreading and potential therapeutics. PLoS Pathog **9:**e1003565. http://dx.doi.org/10.1371/journal.ppat.1003565.

42. **Smith EC, Case JB, Blanc H, Isakov O, Shomron N, Vignuzzi M, Denison MR.** 2015. Mutations in coronavirus nonstructural protein 10 decrease virus replication fidelity. J Virol **89:**6418–6426. http://dx.doi.org /10.1128/JVI.00110-15.

43. **Graham RL, Becker MM, Eckerle LD, Bolles M, Denison MR, Baric RS.** 2012. A live, impaired-fidelity coronavirus vaccine protects in an aged, immunocompromised mouse model of lethal disease. Nat Med **18:**1820–1826. http://dx.doi.org/10.1038/nm.2972.

44. **Campagnola G, McDonald S, Beaucourt S, Vignuzzi M, Peersen OB.** 2014. Structure-function relationships underlying the replication fidelity of viral RNA-dependent RNA polymerases. J Virol **89:**275–286. http://dx .doi.org/10.1128/JVI.01574-14.

45. **Airaksinen A.** 2003. Curing of foot-and-mouth disease virus from persistently infected cells by ribavirin involves enhanced mutagenesis. Virology **311:**339–349. http://dx.doi.org/10.1016/S0042-6822(03)00144-2.

46. **Koonin EV.** 1991. Similarities in RNA helicases. Nature **352:**290–290. http://dx.doi.org/10.1038/352290b0.